Please cite this article in press as: Jabak et al., Left versus right: Exploring the effects of chiral threading intercalators using optical tweezers, Biophysical Journal (2022), https://doi.org/10.1016/j.bpj.2022.04.025

Biophysical *Journal*
Article

Biophysical Society

Left versus right: Exploring the effects of chiral threading intercalators using optical tweezers

Adam A. Jabak,[1] Nicholas Bryden,[1] Fredrik Westerlund,[2] Per Lincoln,[3] Micah J. McCauley,[4] Ioulia Rouzina,[5] Mark C. Williams,[4,*] and Thayaparan Paramanathan[1,*]

[1]Department of Physics, Photonics and Optical Engineering, Bridgewater State University, Bridgewater, Massachusetts; [2]Department of Biology and Biological Engineering, Chalmers University of Technology, Gothenburg, Sweden; [3]Department of Chemistry and Chemical Engineering, Chalmers University of Technology, Gothenburg, Sweden; [4]Department of Physics, Northeastern University, Boston, Massachusetts; and [5]Department of Chemistry and Biochemistry, The Ohio State University, Columbus, Ohio

ABSTRACT Small-molecule DNA-binding drugs have shown promising results in clinical use against many types of cancer. Understanding the molecular mechanisms of DNA binding for such small molecules can be critical in advancing future drug designs. We have been exploring the interactions of ruthenium-based small molecules and their DNA-binding properties that are highly relevant in the development of novel metal-based drugs. Previously we have studied the effects of the right-handed binuclear ruthenium threading intercalator $\Delta\Delta$-[μ-bidppz(phen)$_4$Ru$_2$]$^{4+}$, or $\Delta\Delta$-P for short, which showed extremely slow kinetics and high-affinity binding to DNA. Here we investigate the left-handed enantiomer $\Lambda\Lambda$-[μ-bidppz(phen)$_4$Ru$_2$]$^{4+}$, or $\Lambda\Lambda$-P for short, to study the effects of chirality on DNA threading intercalation. We employ single-molecule optical trapping experiments to understand the molecular mechanisms and nanoscale structural changes that occur during DNA binding and unbinding as well as the association and dissociation rates. Despite the similar threading intercalation binding mode of the two enantiomers, our data show that the left-handed $\Lambda\Lambda$-P complex requires increased lengthening of the DNA to thread, and it extends the DNA more than double the length at equilibrium compared with the right-handed $\Delta\Delta$-P. We also observed that the left-handed $\Lambda\Lambda$-P complex unthreads three times faster than $\Delta\Delta$-P. These results, along with a weaker binding affinity estimated for $\Lambda\Lambda$-P, suggest a preference in DNA binding to the chiral enantiomer having the same right-handed chirality as the DNA molecule, regardless of their common intercalating moiety. This comparison provides a better understanding of how chirality affects binding to DNA and may contribute to the development of enhanced potential cancer treatment drug designs.

SIGNIFICANCE An understanding of the interaction of small ligands with nucleic acids is important for the development of chemicals for therapeutic, biotechnological, and diagnostic purposes. In addition to their importance for biomedicine and biotechnology, DNA-small molecule interactions also serve as models for more complex biological interactions because the specific binding modes exhibited by small molecules are often components of protein-DNA interactions. Here we probe the importance of chirality in determining the fundamental DNA interaction properties. We quantitatively characterize the consequences of altering the chirality of a DNA threading intercalator, demonstrating a vastly different energy landscape for binding. These results show that molecular chirality is a valuable tool for tuning DNA-ligand interactions, which may be used for rational design of anti-cancer drugs.

INTRODUCTION

Since their discovery, small-molecule DNA-binding drugs have had major roles in cancer therapy (1,2). Intercalators are one class of these molecules that have flat planar aromatic regions and bind to DNA by inserting them between the base pairs (3). This stacking alters the structure of double-stranded DNA (dsDNA) and stabilizes it (3–5). Such molecules may act as roadblocks to helicases, preventing DNA replication (6), may prevent the progression of RNA polymerase during transcription (7), or may inhibit topoisomerase (8), all important targets in modern cancer therapy.

Over the past few decades, significant interest in studying ruthenium-based small-molecule complexes has increased

Submitted January 27, 2022, and accepted for publication April 20, 2022.

*Correspondence: mark@neu.edu or thaya@bridgew.edu

Present address: A.A.J. currently at Department of Biochemistry and Molecular Biophysics, University of Pennsylvania, Philadelphia, PA. N.B. currently at Department of Physics and Astronomy, University of North Carolina at Chapel Hill, Chapel Hill, NC.

Editor: Jie Yan.

https://doi.org/10.1016/j.bpj.2022.04.025

Please cite this article in press as: Jabak et al., Left versus right: Exploring the effects of chiral threading intercalators using optical tweezers, Biophysical Journal (2022), https://doi.org/10.1016/j.bpj.2022.04.025

due to the success of other transition metal-based drugs such as cisplatin. Cisplatin is a platinum-based drug that reached clinical trials in the 1970s (9–11) as an antitumor agent (12–14) and is currently used as one of the most prominent chemotherapy drugs (15). Related molecules such as phenanthriplatin have also shown some promise (16–18). The success of these transition metal-based compounds has led to the development of potential ruthenium-based anti-cancer drugs such as NAMI-A, TLD-1433, and KP1019 and its water-soluble sodium salt IT-139, also known as BOLD-100, which has recently been shown to have anti-severe acute respiratory syndrome coronavirus-2 (SARS-CoV-2) activity (19), all of which have reached clinical trials (20–23). Some substitution-inert polypyridyl ruthenium complexes initially studied in the 1980s were shown to bind to DNA with high affinity through intercalation (24), sparking interest in further studies of these complexes. Various designs of ruthenium-based complexes differing by their intercalating moieties were investigated (25) and among these designs the complexes containing dipyridophenazine (dppz) intercalating moieties exhibited the highest affinity to DNA (26). Additionally, two designs of these mononuclear ruthenium intercalators having dppz moieties along with phenanthroline (phen) ancillary ligands, the left-handed Λ-$[Ru(phen)_2dppz]^{2+}$ and right-handed Δ-$[Ru(phen)_2dppz]^{2+}$, were both shown in ensemble studies to have high affinity to binding DNA with distinct stereoselective modes (27,28). These results were later supported by structural studies reporting the x-ray crystal structure of them bound to DNA (29). Furthermore, later modifications made by covalently combining two of these metal-organic ruthenium complexes to form binuclear complexes showed an even higher binding affinity for DNA (30). Such complexes are known as threading intercalators and bind to DNA through a special form of intercalation; they must thread one of their bulky ruthenium-based ends between the two strands that form dsDNA to intercalate the middle planar section sandwiched between two neighboring base pairs to reach the final intercalated binding mode (31–33), which requires the opening of DNA base pairs (34). Threading intercalators have been shown to bind with extremely high affinity to DNA, having dissociation constants in the nanomolar range, and distinctly slower dissociation kinetics, with dissociation occurring in the range of hours to days (5,35).

We have previously used optical tweezers to explore the DNA-binding properties of the two binuclear ruthenium complexes with dppz moieties ΔΔ-$[\mu\text{-bidppz(phen)}_4Ru_2]^{4+}$ (ΔΔ-P) and ΔΔ-$[\mu\text{-bidppz(bpy)}_4Ru_2]^{4+}$ (ΔΔ-B), differing only by their ancillary ligands being either phen or bipyridine (bpy). Our single-molecule measurements indicated that the binding affinities of the two complexes were the same, while a comparison of the binding kinetics revealed faster kinetics for the smaller ΔΔ-B, and an analysis of the structural changes that the DNA undergoes during each binding event supported entirely different binding mechanisms (36,37). Yet both of these complexes had the same right-handed chirality and previous data from ensemble experiments using circular dichroism and luminescence analysis elucidated the possibility of stereoselectivity playing a role in the molecular mechanisms for DNA binding of such threading intercalators (33,38). Here we use optical tweezers to trap single DNA molecules to investigate the DNA-binding properties of the left-handed binuclear ruthenium threading intercalator ΛΛ-$[\mu\text{-bidppz(phen)}_4Ru_2]^{4+}$, or ΛΛ-P for short (Fig. 1 *A*), to compare it with the previously studied right-handed ΔΔ-P (Fig. 1 *A*). Characterizing the binding properties of these enantiomers provides insight into the effects of chirality on DNA binding.

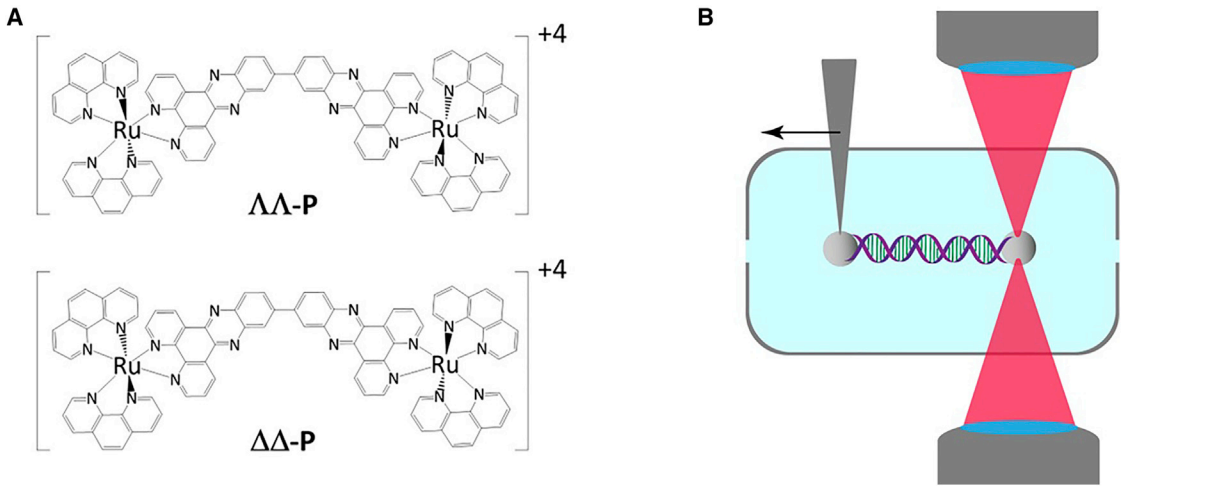

FIGURE 1 Binuclear ruthenium enantiomers and optical tweezers. (*A*) The chemical structures of the binuclear ruthenium complexes ΛΛ-P (*top*) and ΔΔ-P (*bottom*). (*B*) Schematic showing a single DNA molecule tethered between two polystyrene beads and stretched in the dual-beam optical tweezers setup used in the experiments. To see this figure in color, go online.

Please cite this article in press as: Jabak et al., Left versus right: Exploring the effects of chiral threading intercalators using optical tweezers, Biophysical Journal (2022), https://doi.org/10.1016/j.bpj.2022.04.025

MATERIALS AND METHODS

All experiments were conducted in custom-built homemade flow chambers (~100 μL volume) at room temperature (21°C) using a dual-beam optical tweezers setup as previously described (39). In short, two finely focused counter-propagating laser beams (wavelength 830 nm) were used to trap a single bacteriophage λ-DNA (contour length of 48,502 bp) biotinylated at the 3′ ends. The DNA molecule was tethered between two streptavidin-coated polystyrene beads (~3 μm diameter): one bead was caught in the optical trap while the other was affixed to a micropipette tip (1 μm diameter) attached to the flow chamber through suction (Fig. 1 *B*). The torsionally unconstrained tethered DNA molecule could be held at a constant force (±1 pN) by precisely manipulating a piezoelectric controlled stage through a force feedback loop to move the micropipette in small steps (±10 nm). DNA stretching curves were obtained for each molecule to ensure only a single molecule was present (black curve in Fig. 2 *A*). The tethered molecule was then stretched and held at a constant force (34) while the ligand was introduced in the chamber at a constant flow rate (~2 μL/s). The binding of ligand to DNA was measured as the DNA molecule extended while maintaining constant force, until reaching equilibrium. The flow of ligand was then switched to buffer and the DNA extension returned as ligand washed out; the molecule was then discarded. These association and dissociation constant-force experiments were repeated at five different concentrations at each force with at least three DNA molecules for each concentration. The whole process described above was done at 20, 30, 40, and 50 pN constant forces. All experiments were conducted under buffer conditions of 10 mM Tris, 100 mM NaCl, and pH 8. The ΛΛ-P complex was synthesized as described elsewhere (40).

RESULTS

ΛΛ-P exhibits slow binding kinetics

Constant-force measurements of ΛΛ-P binding, where a single DNA molecule is held at a particular force as mentioned in the section "materials and methods," yield slow binding kinetics. Constant-force measurements performed at 20 pN force in the presence of various concentrations of ΛΛ-P and the resulting kinetics are presented in Fig. 2. A representative curve showing the extension of the DNA molecule when held at 20 pN constant force while flowing 20 nM ΛΛ-P is illustrated in Fig. 2 *A*. These extensions measured at various concentrations of ΛΛ-P can be represented as a function of time (open circles in Fig. 2 *B*) and fit (solid lines in Fig. 2 *B*) to the single exponential model shown in Eq. 1:

$$L(t) = L_0 + (L_{eq} - L_0)(1 - e^{-k_{tot}t}), \quad (1)$$

where L_0 is the length of DNA in absence of ligand at that force, L_{eq} is the length at ligand-bound equilibrium, and $k_{tot}(F, C)$ is the total rate of binding at a specific force F and concentration C. After the binding of ligand reached equilibrium, the flow of ligand was switched to buffer, and the length decrease as a function of time (open circles in Fig. 2 *C*) was measured as ligand washed off. These measurements were fit (solid lines in Fig. 2 *C*) to a single exponential model shown in Eq. 2 below:

$$L(t) = (L_{eq} - L_0)e^{-k_{off}t} + L_0, \quad (2)$$

where $k_{off}(F, C)$ is the estimated dissociation rate. At least three separate DNA molecules were used to obtain an average of total rates for each concentration at 20 pN constant-force experiments (blue data points in Fig. 2 *D*). Since the total rates obtained for each concentration are a sum of the on and off rates, k_{on} and k_{off}, and the on rate is concentration dependent, the association rate k_a for 20 pN can be estimated using the following linear relationship:

$$k_{tot} = k_a C + k_{off}. \quad (3)$$

This yields an association rate of (2.3 ± 0.4) $\times 10^{-5}$ $M^{-1}s^{-1}$ and off rate 0.0065 ± 0.0009 s^{-1} at 20 pN. The average dissociation rate obtained from washing experiments (red data points in Fig. 2 *D*), 0.0059 ± 0.0007 s^{-1}, agrees well with the value obtained from the fit described in Eq. 3 within the uncertainties.

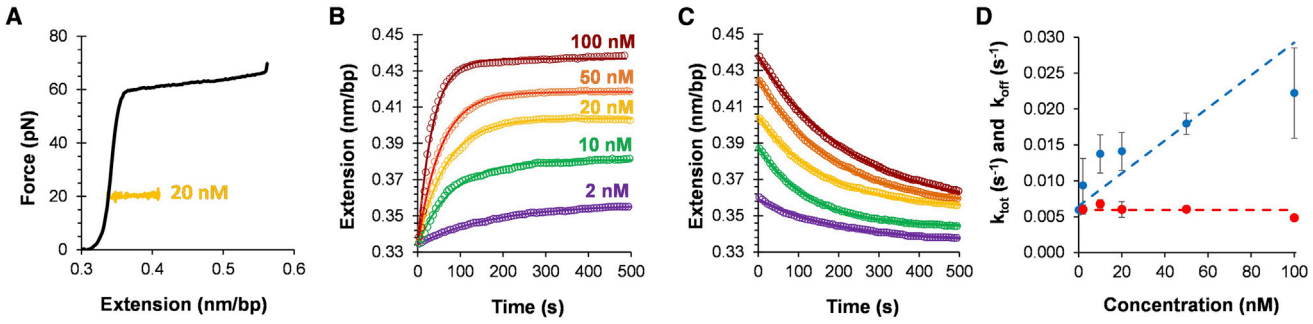

FIGURE 2 Threading and unthreading at 20 pN constant force. (*A*) Representative curve of DNA stretching in the absence of the ligand (*black*) and a DNA stretched and held at 20 pN constant force while flowing 20 nM ΛΛ-P (*orange*). (*B*) Representative curves of DNA extension measured as a function of time while increasing concentrations of ΛΛ-P thread through DNA held at 20 pN. Open circles represent the data and solid lines represent the corresponding single exponential fits of Eq. 1. (*C*) Representative curves showing the extension decrease as a function of time while washing away ΛΛ-P with buffer after reaching equilibrium at concentrations shown in (*B*). Open circles represent the data and solid lines represent the corresponding single exponential fits of Eq. 2. (*D*) Average total rates obtained from at least three experiments at various concentrations of ΛΛ-P (*blue circles*) fit to linear dependency on concentrations expressed by Eq. 3 (*blue dashed line*). The average off rates obtained from at least three washing experiments (*red circles*) and the average of these off rates (*red dashed line*). The error bars indicate the standard deviation of the averages.

Please cite this article in press as: Jabak et al., Left versus right: Exploring the effects of chiral threading intercalators using optical tweezers, Biophysical Journal (2022), https://doi.org/10.1016/j.bpj.2022.04.025

Force facilitates the DNA threading and unthreading of ΛΛ-P

As previously demonstrated for 20 pN constant force, the k_a was also obtained from the total rate for 30, 40, and 50 pN constant-force measurements (Fig. S1). The association rates observed (green data points in Fig. 3 *A*) were found to be exponentially facilitated by force. These values were fit to Eq. 4 (green dashed line Fig. 3 *A*) to obtain the association rate in the absence of force, $k_a(0)$, and the lengthening required for a single threading event, x_{on}:

$$k_a(F) = k_a(0)\exp\left(\frac{Fx_{on}}{k_BT}\right), \tag{4}$$

where k_B is the Boltzmann constant and T is the temperature at which experiments were conducted (21°C). From this fitting we obtain $k_a(0)$ to be (8.2 ± 2.6) $\times 10^3$ $M^{-1}s^{-1}$ and x_{on} to be 0.58 ± 0.02 nm.

Similarly, the average of measured off rates ($k_{off}(F)$) obtained from dissociation experiments at each force (red data points in Fig. 3 *B*), were also exponentially facilitated by force as described by Eq. 5:

$$k_{off}(F) = k_{off}(0)\exp\left(\frac{Fx_{off}}{k_BT}\right), \tag{5}$$

where $k_{off}(0)$ is the dissociation rate in the absence of force and x_{off} is the lengthening required for a single unthreading event. From this fitting (red dashed line in Fig. 3 *B*) we obtain $k_{off}(0)$ to be (3.5 ± 0.5) $\times 10^{-3}$ s^{-1} and x_{off} to be 0.09 ± 0.02 nm.

Using the quotient of L_{eq} values obtained from the single exponential fits in the association experiments (Fig. 2 *B*) we can calculate the fractional binding θ (F, C) for a particular concentration at a certain force (Eq. 6):

$$\theta(F,C) = \frac{\Delta L_{eq}}{\Delta L_{sat}} = \frac{L_{eq}(F,C) - L_0(F)}{L_{sat}(F) - L_0(F)}, \tag{6}$$

where $L_0(F)$ is the length of the DNA in the absence of ΛΛ-P at a particular force and $L_{sat}(F)$ is the lengthening at saturated concentrations of ΛΛ-P at that force. The fractional binding was fit to the McGhee-von Hippel isotherm (MGVH) (41,42), a one-dimensional lattice-binding model (Eq. 7):

$$\theta(K_d,n) = \frac{C}{K_d}\left[\frac{n(1-\theta)^n}{\left(1-\theta+\frac{\theta}{n}\right)^{n-1}}\right], \tag{7}$$

where n is the binding site size and K_d is the dissociation constant for each force. Fig. 3 *C* illustrates the average equilibrium extensions measured for various concentrations from constant-force experiments fit to MGVH at the four different forces. The K_d values obtained for each force from MGVH analysis (Fig. 3 *D*) can be extrapolated to zero force using Eq. 8 to obtain the force independent dissociation constant $K_d(0)$ and the equilibrium lengthening of DNA upon a single intercalation event Δx_{eq}:

$$K_d(F) = K_d(0)\exp\left(\frac{-F\Delta x_{eq}}{k_BT}\right). \tag{8}$$

We obtain the dissociation constant in the absence of force, $K_d(0)$, to be 838 ± 186 nM and Δx_{eq} to be 0.48 ± 0.03 nm. After performing chi-square minimization, a binding site size of $n = 5$ was used in the above MGVH fits to keep the fitting parameters to a minimum number. The value $n = 5$ agrees well within the uncertainty, with the expected relationship $\Delta x_{eq} = n(F)\Delta L_{sat}(F)$ (43), between the obtained Δx_{eq} from kinetics and measured saturation lengths $\Delta L_{sat}(F)$ fit to the worm-like chain model (WLC, Fig. 4) in Eq. 9 below (44):

$$L_{sat} = b\left(1 - \frac{1}{2}\left(\frac{k_BT}{Fp}\right)^{\frac{1}{2}} + \frac{F}{s}\right), \tag{9}$$

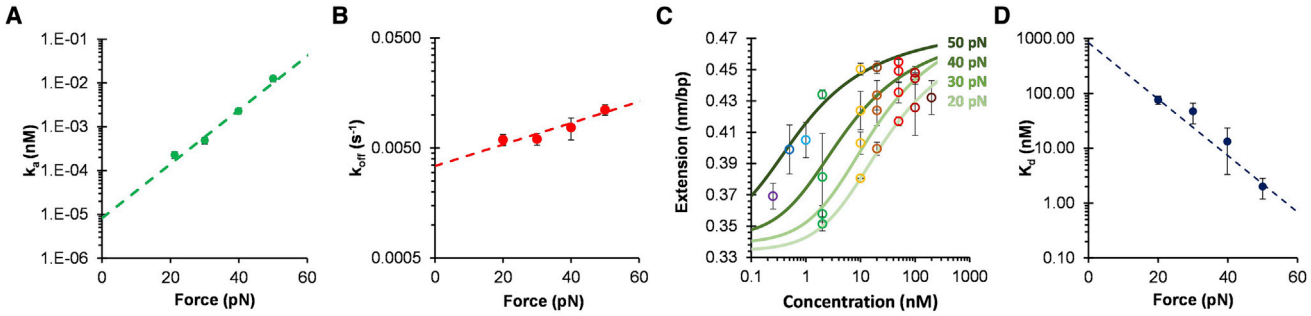

FIGURE 3 Force-dependent binding properties. (*A*) Association rates obtained from the constant-force experiments (*green circles*) fit to exponential dependency on force expressed by Eq. 4 (*green dashed line*). (*B*) Dissociation rates obtained at various forces (*red circles*) fit to exponential dependency on force expressed by Eq. 5 (*red dashed line*). (*C*) McGhee-von Hippel (MGVH) fits expressed by Eq. 7 (*solid lines*, different colors represent different forces) of the fractional binding obtained at different forces (*open circles*, different colors represent different concentrations). (*D*) Force dependence of the dissociation constants obtained from MGVH fits (*blue circles*) extrapolated according to Eq. 8 (*blue dashed line*) to obtain the binding affinity in the absence of force. The error bars indicate the standard deviations of the averages.

Please cite this article in press as: Jabak et al., Left versus right: Exploring the effects of chiral threading intercalators using optical tweezers, Biophysical Journal (2022), https://doi.org/10.1016/j.bpj.2022.04.025

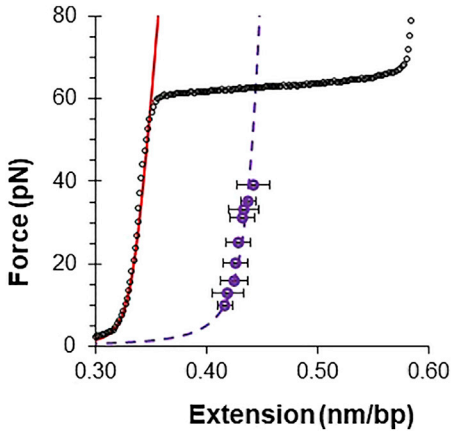

FIGURE 4 WLC model fits. The DNA stretching curve (*black*) fit to the WLC model (*red*) described by Eq. 9 and DNA saturated with ΛΛ-P (*purple circles*) fit to the WLC (*purple dashed line*). The error bars indicate the standard deviations of the averages. To see this figure in color, go online.

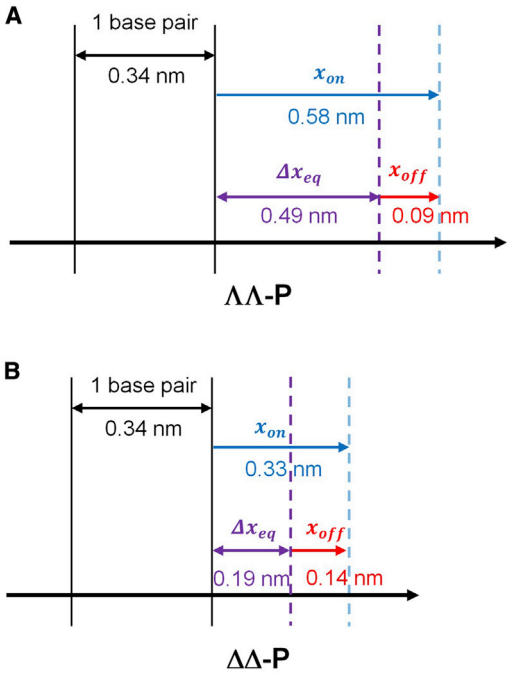

FIGURE 5 Comparison of the DNA structural changes during the threading and unthreading of the chiral enantiomers. (*A*) A DNA base pair (*black*) has to be extended to facilitate the threading of ΛΛ-P (*blue arrow*), relaxes back to equilibrium (*purple arrow*), and has to be extended again to facilitate unthreading (*red arrow*). (*B*) The same description in (*A*) but for ΔΔ-P adapted from (36). To see this figure in color, go online.

where b is the contour length (0.44 ± 0.01 nm/bp), p is the persistence length (25 ± 9 nm), and s is the stretch modulus (1493 ± 808 pN) of the ligand-bound DNA molecule.

To further buttress our prior estimation of the dissociation constant K_d, it can also be estimated using the quotient of off rates and association rates extrapolated to zero force measured in the kinetics experiments, $K_d(0) = k_{off}(0)/k_a(0)$, which gives us an estimate in the same order of magnitude (427 ± 148 nM).

DISCUSSION

The results quantifying ΛΛ-P binding strength, kinetics, and structural changes that DNA must undergo for each intercalating event are tabulated against those of the previously studied ΔΔ-P enantiomer (36) in Table 1.

We have shown that DNA threading by ΛΛ-P is strongly dependent on force, indicated by the exponential decrease of the dissociation constant K_d with increasing force (Fig. 3 *D*), just as ΔΔ-P (36). Interestingly, the left-handed ΛΛ-P molecules exhibit an almost 20-fold weaker binding (i.e., higher value for K_d) compared with their right-handed sibling ΔΔ-P, despite both molecules having common intercalating dppz moieties. This lower binding affinity, which is unexpected because the intercalating moieties are the same, may be an effect of the opposite left-handed chiral ligands of ΛΛ-P sterically not fitting well with the right-handed DNA molecule in the intercalated binding mode. Thus, the auxiliary ligands affect the binding pocket in different ways for these two enantiomers. The importance of steric fit of the ligand into the DNA structure over the nature of intercalating moiety is further validated by the similar binding affinity observed previously for ΔΔ-P and ΔΔ-B (37), both having the same chirality but with different ancillary ligands.

TABLE 1 Comparison of the DNA-binding properties and kinetics of ΛΛ-P and ΔΔ-P (36)

Binding properties	ΛΛ-P	ΔΔ-P
K_d (0) (nM)	838 ± 186	44 ± 2
k_a (0) ($M^{-1}s^{-1}$)	(8.2 ± 2.6) × 10^3	(10.1 ± 0.1) x10^3
k_{off} (0) (s^{-1})	(3.5 ± 0.5) × 10^{-3}	(1.4 ± 0.1) x10^{-3}
Δx_{eq} (nm)	0.48 ± 0.03	0.19 ± 0.01
x_{on} (nm)	0.58 ± 0.02	0.33 ± 0.01
x_{off} (nm)	0.09 ± 0.02	0.14 ± 0.01

Examining the threading kinetics into DNA, we measured the association rate k_a of ΛΛ-P (8.2 ± 2.6) ×10^3 $M^{-1}s^{-1}$ to be slightly slower, but of the same order of magnitude, as its previously studied enantiomer ΔΔ-P (10.1 ± 0.1) ×10^3 $M^{-1}s^{-1}$. This result conflicts with previous measurements from luminescence and circular dichroism (CD) experiments (38,45). The CD measurements suggest a multi-exponential fitting of the threading kinetics: tri-exponential for ΛΛ-P and bi-exponential for ΔΔ-P (38), which may reflect the kinetics of additional non-intercalating binding steps that do not change DNA length and are therefore not detected here. The force-facilitated binding of ΛΛ-P in our experiments and ΔΔ-P in previous (36) are both well described by a single

exponential dependence on time, leading to zero force rates within the same order of magnitude. The off rate in the absence of force, or the unthreading rate, of ΛΛ-P $(3.5 \pm 0.5) \times 10^{-3}$ s^{-1} is also in the same order but a little faster than ΔΔ-P $(1.4 \pm 0.1) \times 10^{-3}$ s^{-1}. This similarity in the binding kinetics of the pair of enantiomers suggests that the chirality change of ancillary ligands does not drastically affect how fast these enantiomers thread or unthread DNA.

Despite the comparable binding kinetics in the absence of force, the structural changes that DNA undergoes to thread and unthread these enantiomers vary drastically. The DNA elongation required for threading a single ΛΛ-P ligand, x_{on} (0.58 ± 0.02 nm), is much larger than for ΔΔ-P (0.33 ± 0.01 nm), suggesting that the left-handed ancillary ligands require more space to thread. The equilibrium elongation Δx_{eq} of the DNA for each intercalation event is more than double for ΛΛ-P (0.48 ± 0.03 nm) compared with ΔΔ-P (0.19 ± 0.01 nm). This is likely an effect of the opposing chirality of the left-handed ancillary ligands of ΛΛ-P not fitting well in right-handed DNA due to steric hindrance. Previous examination of the binding modes of ΛΛ-P, ΔΔ-P, and the meso ΔΛ-P stereoisomers indicates that, for all three stereoisomers, the Ru coordinated to the intercalated dppz moiety resides deep in the minor groove, and that for ΔΛ-P the Λ moiety is in the minor groove and the Δ moiety in the major groove (33,40). It also has been suggested that profound structural changes are necessary for these ligands to bind DNA, especially such as the opening of at least one base pair (40). The DNA elongation required for the unthreading of each ΛΛ-P ligand, x_{off} (0.09 ± 0.02 nm), indicates a need to elongate the base pairs by 0.09 nm further than the equilibrium extension to unthread ΛΛ-P, which is less than the elongation required for ΔΔ-P (0.14 ± 0.01 nm), possibly explaining the slightly faster off rates measured for ΛΛ-P compared with ΔΔ-P. In addition, the equilibrium extension Δx_{eq} obtained from MGVH for ΛΛ-P (0.48 ± 0.03 nm) agrees well with the Δx_{eq} (0.49 ± 0.03 nm) obtained using the difference between x_{on} and x_{off} obtained from the kinetics measurements. These structural changes required for ΛΛ-P binding suggest a locking mechanism similar to the previously studied ΔΔ-P (Fig. 5), but with much greater associated length changes.

High affinity and slow kinetics when binding to DNA are crucial properties of small-molecule applications for tumor treatment (46,47). Quantitative analysis of the two chiral enantiomers ΛΛ-P and ΔΔ-P suggest that they have these properties as well as the same binding mode to DNA. Notwithstanding, the deformations needed to thread and unthread DNA favor the right-handed ΔΔ-P with smaller elongations required for threading and longer elongations required for unthreading, making it a more stable threading intercalator as previously revealed (48). These results demonstrate that chirality plays a significant role in the mechanism by which these enantiomers bind to and distort DNA structure. Therefore, chirality can be used as a powerful tool to tune the energy landscape of DNA intercalation, which may play a substantial role in improving the designs of anti-cancer drugs.

SUPPORTING MATERIAL

Supporting material can be found online at https://doi.org/10.1016/j.bpj.2022.04.025.

AUTHOR CONTRIBUTIONS

A.A.J. performed constant-force measurements at 40 and 50 pN, performed saturation experiments, and analyzed the data. N.B. performed constant-force measurements at 20 and 30 pN and analyzed the data. F.W. and P.L. contributed reagents and interpreted the data. M.J.M. contributed reagents. I.R. analyzed and interpreted the data. M.C.W. and T.P. designed research, and analyzed and interpreted the data. All authors contributed to writing the manuscript.

DECLARATION OF INTERESTS

The authors declare no conflict of interest.

ACKNOWLEDGMENTS

This research was funded by National Science Foundation grant MCB-1817712 (to M.C.W. and T.P.), Adrian Tinsley Program, and Bartlett's Internship (to N.B. and A.A.J.) at Bridgewater State University.

REFERENCES

1. Hurley, L. H. 2002. DNA and its associated processes as targets for cancer therapy. *Nat. Rev. Cancer.* 2:188–200. https://doi.org/10.1038/nrc749. https://www.ncbi.nlm.nih.gov/pubmed/11990855.

2. Wheate, N. J., C. R. Brodie, …, J. R. Aldrich-Wright. 2007. DNA intercalators in cancer therapy: organic and inorganic drugs and their spectroscopic tools of analysis. *Mini Rev. Med. Chem.* 7:627–648. https://doi.org/10.2174/138955707780859413. https://www.ncbi.nlm.nih.gov/pubmed/17584161.

3. Lerman, L. 1961. Structural considerations in the interaction of DNA and acridines. *J. Mol. Biol.* 3:18–IN14. https://doi.org/10.1016/s0022-2836(61)80004-1.

4. McCauley, M. J., and M. C. Williams. 2009. Optical tweezers experiments resolve distinct modes of DNA-protein binding. *Biopolymers.* 91:265–282. https://doi.org/10.1002/bip.21123.

5. Almaqwashi, A. A., T. Paramanathan, …, M. C. Williams. 2016. Mechanisms of small molecule-DNA interactions probed by single-molecule force spectroscopy. *Nucleic Acids Res.* 44:3971–3988. https://doi.org/10.1093/nar/gkw237. https://www.ncbi.nlm.nih.gov/pubmed/27085806.

6. Lian, C., H. Robinson, and A. H.-J. Wang. 1996. Structure of actinomycin D bound with $(GAAGCTTC)_2$ and $(GATGCTTC)_2$ and its binding to the $(CAG)_n$:$(CTG)_n$ triplet sequence as determined by NMR analysis. *J. Am. Chem. Soc.* 118:8791–8801. https://doi.org/10.1021/ja961631p.

7. Waring, M. J. 1981. DNA modification and cancer. *Annu. Rev. Biochem.* 50:159–192. https://doi.org/10.1146/annurev.bi.50.070181.001111.

Please cite this article in press as: Jabak et al., Left versus right: Exploring the effects of chiral threading intercalators using optical tweezers, Biophysical Journal (2022), https://doi.org/10.1016/j.bpj.2022.04.025

8. Atwal, M., R. L. Swan, …, C. A. Austin. 2019. Intercalating TOP2 poisons attenuate topoisomerase action at higher concentrations. *Mol. Pharmacol.* 96:475–484. https://doi.org/10.1124/mol.119.117259.
9. Murry, D. J. 1997. Comparative clinical pharmacology of cisplatin and carboplatin. *Pharmacother. J. Hum. Pharmacol. Drug Ther.* 17:140S–145S.
10. Loehrer, P. J., and L. H. Einhorn. 1984. Cisplatin. *Ann. Intern. Med.* 100:704–713. https://doi.org/10.7326/0003-4819-100-5-704.
11. Higby, D. J., D. J. Higby, J. F. Holland…, 1974. Diaminodichloroplatinum: a phase I study showing responses in testicular and other tumors. *Cancer.* 33:1219–1225.
12. Rosenberg, B., L. Van Camp, and T. Krigas. 1965. Inhibition of cell division in Escherichia coli by electrolysis products from a platinum electrode. *Nature.* 205:698–699. https://doi.org/10.1038/205698a0.
13. Rosenberg, B., L. VanCamp, J. E. Trosko, and V. H. Mansour. 1969. Platinum compounds: a new class of potent antitumour agents. *Nature.* 222:385–386. https://doi.org/10.1038/222385a0. https://www.ncbi.nlm.nih.gov/pubmed/5782119.
14. Benjamin Garbutcheon-Singh, K., K. B. Garbutcheon-Singh, …, J. R. Aldrich-Wright. 2011. Transition metal based anticancer drugs. *Curr. Top. Med. Chem.* 11:521–542. https://doi.org/10.2174/156802611794785226. https://www.ncbi.nlm.nih.gov/pubmed/21189131.
15. Brown, A., S. Kumar, and P. B. Tchounwou. 2019. Cisplatin-based chemotherapy of human cancers. *J. Cancer Sci. Ther.* 11:97.
16. Park, G. Y., J. J. Wilson, …, S. J. Lippard. 2012. Phenanthriplatin, a monofunctional DNA-binding platinum anticancer drug candidate with unusual potency and cellular activity profile. *Proc. Natl. Acad. Sci. U. S. A.* 109:11987–11992. https://doi.org/10.1073/pnas.1207670109.
17. Zhou, W., M. Almeqdadi, …, S. J. Lippard. 2018. The effect of geometric isomerism on the anticancer activity of the monofunctional platinum complex. *Chem. Commun.* 54:2788–2791.
18. Almaqwashi, A. A., W. Zhou, …, M. C. Williams. 2019. DNA intercalation facilitates efficient DNA-targeted covalent binding of phenanthriplatin. *J. Am. Chem. Soc.* 141:1537–1545. https://doi.org/10.1021/jacs.8b10252.
19. Munteanu, A.-C., and V. Uivarosi. 2021. Ruthenium complexes in the fight against pathogenic microorganisms. An extensive review. *An Extensive Rev. Pharmaceutics.* 13:874. https://doi.org/10.3390/pharmaceutics13060874.
20. Hartinger, C. G., S. Zorbas-Seifried, …, B. K. Keppler. 2006. From bench to bedside–preclinical and early clinical development of the anticancer agent indazolium trans-[tetrachlorobis (1H-indazole) ruthenate (III)](KP1019 or FFC14A). *J. Inorg. Biochem.* 100:891–904. https://doi.org/10.1016/j.jinorgbio.2006.02.013.
21. Sava, G., E. Alessio, …, G. Mestroni. 1999. Sulfoxide ruthenium complexes: non-toxic tools for the selective treatment of solid tumour metastases. *In* Metallopharmaceuticals I. Springer, pp. 143–169.
22. Monro, S., K. L. Colón, …, S. A. McFarland. 2018. Transition metal complexes and photodynamic therapy from a tumor-centered approach: challenges, opportunities, and highlights from the development of TLD1433. *Chem. Rev.* 119:797–828. https://doi.org/10.1021/acs.chemrev.8b00211.
23. Trondl, R., P. Heffeter, …, B. K. Keppler. 2014. NKP-1339, the first ruthenium-based anticancer drug on the edge to clinical application. *Chem. Sci.* 5:2925–2932. https://doi.org/10.1039/c3sc53243g.
24. Barton, J. K., A. Danishefsky, and J. Goldberg. 1984. Tris (phenanthroline) ruthenium (II): stereoselectivity in binding to DNA. *J. Am. Chem. Soc.* 106:2172–2176. https://doi.org/10.1021/ja00319a043.
25. Mihailovic, A., I. Vladescu, …, M. E. Nuñez. 2006. Exploring the interaction of ruthenium (II) polypyridyl complexes with DNA using single-molecule techniques. *Langmuir.* 22:4699–4709. https://doi.org/10.1021/la053242r.
26. Vladescu, I. D., M. J. McCauley, …, M. C. Williams. 2007. Quantifying force-dependent and zero-force DNA intercalation by single-molecule stretching. *Nat. Methods.* 4:517–522. https://doi.org/10.1038/nmeth1044. https://www.ncbi.nlm.nih.gov/pubmed/17468764.
27. Haq, I., P. Lincoln, …, J. B. Chaires. 1995. Interaction of. delta.-and. lambda.-[Ru (phen) 2DPPZ] 2+ with DNA: a calorimetric and equilibrium binding study. *J. Am. Chem. Soc.* 117:4788–4796. https://doi.org/10.1021/ja00122a008.
28. Andersson, J., L. H. Fornander, …, P. Lincoln. 2013. Lifetime heterogeneity of DNA-bound dppz complexes originates from distinct intercalation geometries determined by complex–complex interactions. *Inorg. Chem.* 52:1151–1159. https://doi.org/10.1021/ic302626d.
29. Hall, J. P., D. Cook, …, C. J. Cardin. 2013. X-ray crystal structure of rac-[Ru (phen) 2dppz] 2+ with d (ATGCAT) 2 shows enantiomer orientations and water ordering. *J. Am. Chem. Soc.* 135:12652–12659. https://doi.org/10.1021/ja403590e.
30. Lincoln, P., and B. Nordén. 1996. Binuclear ruthenium (II) phenanthroline compounds with extreme binding affinity for DNA. *Chem. Commun.* 18:2145–2146. https://doi.org/10.1039/cc9960002145.
31. Önfelt, B., P. Lincoln, and B. Nordén. 2001. Enantioselective DNA threading dynamics by phenazine-linked [Ru (phen) 2dppz] 2+ dimers. *J. Am. Chem. Soc.* 123:3630–3637. https://doi.org/10.1021/ja003624d.
32. Wilhelmsson, L. M., F. Westerlund, …, B. Nordén. 2002. DNA-binding of semirigid binuclear ruthenium complex Δ, Δ-[μ-(11, 11 '-bidppz)(phen) 4Ru2] 4+: extremely slow intercalation kinetics. *J. Am. Chem. Soc.* 124:12092–12093. https://doi.org/10.1021/ja027252f.
33. Westerlund, F., M. P. Eng, …, P. Lincoln. 2007. Binding geometry and photophysical properties of DNA-threading binuclear ruthenium complexes. *The J. Phys. Chem. B.* 111:310–317. https://doi.org/10.1021/jp065871v.
34. Paramanathan, T., F. Westerlund, …, M. C. Williams. 2008. Mechanically manipulating the DNA threading intercalation rate. *J. Am. Chem. Soc.* 130:3752–3753. https://doi.org/10.1021/ja711303p. https://www.ncbi.nlm.nih.gov/pubmed/18311981.
35. Westerlund, F., P. Nordell, …, P. Lincoln. 2007. Kinetic characterization of an extremely slow DNA binding equilibrium. *J. Phys. Chem. B.* 111:9132–9137. https://doi.org/10.1021/jp072126p.
36. Almaqwashi, A. A., T. Paramanathan, …, M. C. Williams. 2014. Strong DNA deformation required for extremely slow DNA threading intercalation by a binuclear ruthenium complex. *Nucleic Acids Res.* 42:11634–11641. https://doi.org/10.1093/nar/gku859. https://www.ncbi.nlm.nih.gov/pubmed/25245944.
37. Clark, A. G., M. N. Naufer, …, M. C. Williams. 2018. Reshaping the energy landscape transforms the mechanism and binding kinetics of DNA threading intercalation. *Biochemistry.* 57:614–619. https://doi.org/10.1021/acs.biochem.7b01036. https://www.ncbi.nlm.nih.gov/pubmed/29243480.
38. Westerlund, F., P. Nordell, …, P. Lincoln. 2008. Complex DNA binding kinetics resolved by combined circular dichroism and luminescence analysis. *J. Phys. Chem. B.* 112:6688–6694. https://doi.org/10.1021/jp711116z.
39. McCauley, M. J., and M. C. Williams. 2007. Mechanisms of DNA binding determined in optical tweezers experiments. *Biopolymers.* 85:154–168. https://doi.org/10.1002/bip.20622.
40. Wilhelmsson, L. M., E. K. Esbjörner, …, P. Lincoln. 2003. Meso stereoisomer as a probe of enantioselective threading intercalation of semirigid ruthenium complex [μ-(11, 11 '-bidppz)(phen) 4Ru2] 4+. *J. Phys. Chem. B.* 107:11784–11793. https://doi.org/10.1021/jp036302f.
41. McGhee, J. D., and P. H. von Hippel. 1974. Theoretical aspects of DNA-protein interactions: co-operative and non-co-operative binding of large ligands to a one-dimensional homogeneous lattice. *J. Mol. Biol.* 86:469–489. https://www.ncbi.nlm.nih.gov/pubmed/4416620.
42. Kowalczykowski, S. C., L. S. Paul, …, P. H. Von Hippel. 1986. Cooperative and noncooperative binding of protein ligands to nucleic acid lattices: experimental approaches to the determination of thermodynamic parameters. *Biochemistry.* 25:1226–1240. https://doi.org/10.1021/bi00354a006.
43. Almaqwashi, A. A., J. Andersson, …, M. C. Williams. 2016. Dissecting the dynamic pathways of stereoselective DNA threading intercalation. *Biophys. J.* 110:1255–1263. https://doi.org/10.1016/j.bpj.2016.02.016.
44. Odijk, T. 1995. Stiff chains and filaments under tension. *Macromolecules.* 28:7016–7018. https://doi.org/10.1021/ma00124a044.

45. Nordell, P., and P. Lincoln. 2005. Mechanism of DNA threading intercalation of binuclear Ru complexes: uni-or bimolecular pathways depending on ligand structure and binding density. *J. Am. Chem. Soc.* 127:9670–9671. https://doi.org/10.1021/ja0521674.

46. Müller, W., and D. M. Crothers. 1968. Studies of the binding of actinomycin and related compounds to DNA. *J. Mol. Biol.* 35:251–290. https://doi.org/10.1016/s0022-2836(68)80024-5.

47. Howell, L. A., R. Gulam, …, M. Searcey. 2010. Design and synthesis of threading intercalators to target DNA. *Bioorg. Med. Chem. Lett.* 20:6956–6959. https://doi.org/10.1016/j.bmcl.2010.09.128.

48. Andersson, J., M. Li, and P. Lincoln. 2010. AT-Specific DNA binding of binuclear ruthenium complexes at the border of threading intercalation. *Chemistry–A Eur. J.* 16:11037–11046. https://doi.org/10.1002/chem.201000180.

Biophysical Journal, Volume *121*

Supplemental information

Left versus right: Exploring the effects of chiral threading intercalators using optical tweezers

Adam A. Jabak, Nicholas Bryden, Fredrik Westerlund, Per Lincoln, Micah J. McCauley, Ioulia Rouzina, Mark C. Williams, and Thayaparan Paramanathan

Supplementary Information

Left vs. Right: Exploring the Effects of Chiral Threading Intercalators using Optical Tweezers

Adam A. Jabak, Nicholas Bryden, Fredrik Westerlund, Per Lincoln, Micah J. McCauley, Ioulia Rouzina, Mark C. Williams, and Thayaparan Paramanathan

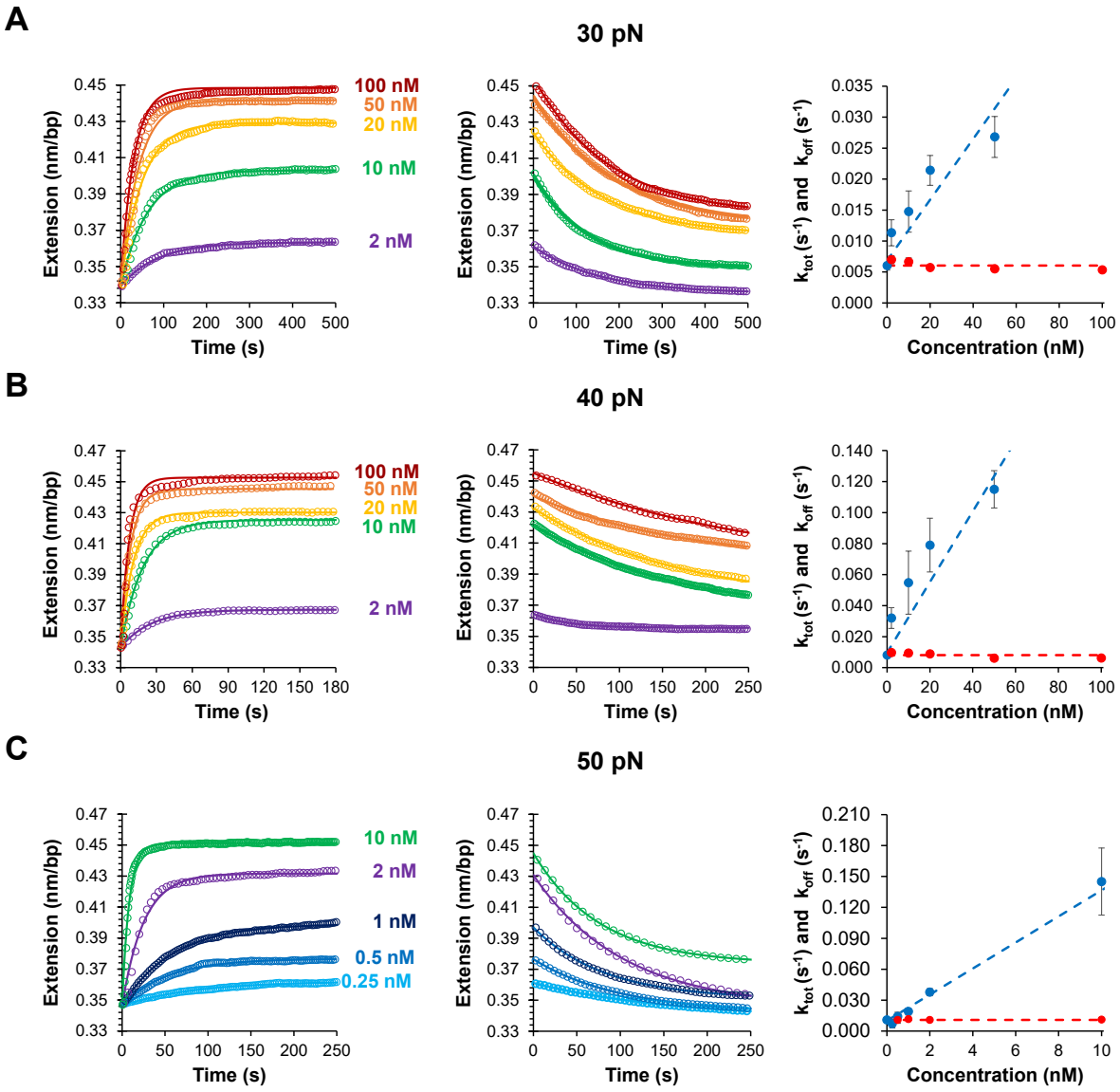

Figure S1: Threading and unthreading at 30, 40, and 50 pN constant force. (A) *Left*: Representative curves of DNA extension measured as function of time while various concentrations of ΛΛ-P thread through DNA held at constant 30 pN force. Open circles represent the data and solid lines represent the corresponding single exponential fittings expressed by Eq. 1. *Center*: Representative curves showing the extension decrease as function of time while washing away ΛΛ-P with buffer after reaching equilibrium at

concentrations shown in left panel. Open circles represent the data and solid lines represent the corresponding single exponential fittings expressed by Eq. 2. *Right*: Average total rates obtained from at least three experiments at various concentrations of ΛΛ-P (blue circles) fit to linear dependency on concentrations expressed by Eq. 3 (blue dashed line). The average off rates obtained from at least three washing experiments (red circles) and the average of these off rates (red dashed line). (B, C) Same as (A) but for 40 and 50 pN constant force.